ACS OMEGA

http://pubs.acs.org/journal/acsodf

Article

Dynamic Dissociation Behaviors of sII Hydrates in Liquid Water by Heating: A Molecular Dynamics Simulation Approach

Peihan Yang, Dongdong Guo, and Bin Fang*

Cite This: *ACS Omega* 2022, 7, 42774−42782

Read Online

ACCESS | Metrics & More | Article Recommendations | Supporting Information

ABSTRACT: An understanding of the dynamic behavior of subtle hydrate dissociation in the liquid water phase is fundamental for gas production from marine hydrate reservoirs. Molecular dynamics simulations are performed in this study to investigate the dissociation kinetics of pure propane and binary propane + methane sII hydrates in a liquid water environment. The results show that faster hydrate dissociation rates are observed at higher initial temperatures. The hydrate phase dissociates from the cluster surface to the inside in a layer-by-layer manner under the simulation temperature conditions, which is similar to the behavior of sI hydrates and is independent of the hydrate crystal type. Compared to the binary sII hydrate, the pure sII hydrate dissociates more easily under the same initial temperature conditions, which can be attributed to the stabilizing effect of guest molecules in the hydrate cages. The empty cages collapse in one step, in contrast to the two-step pathway induced by the guest−host interaction. In addition, a hydrocarbon phase forms in the binary hydrate dissociation system instead of nanobubbles. These results can provide molecular-level insights into the dynamic mechanism of hydrate dissociation and theoretical guidance for gas recovery by thermal injection from marine hydrate reservoirs.

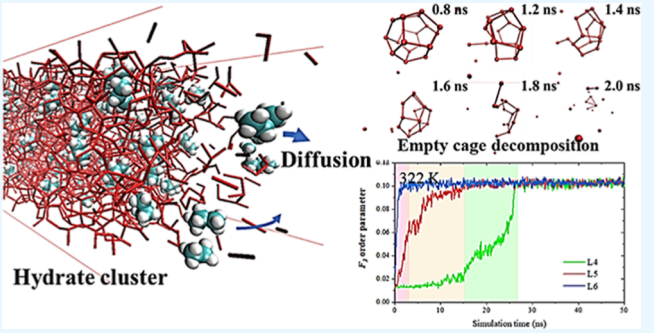

1. INTRODUCTION

Natural gas hydrates (NGHs) are ice-like crystals in which guest molecules (such as CH_4 and C_3H_8) are trapped within cage networks formed by hydrogen-bonded host water molecules at low temperatures and high pressures.[1] In nature, most NGHs occur in permafrost regions and marine sediments, and more than 90% of global NGHs are located in the latter environment.[2] Three typical hydrate crystal structures have been identified (cubic sI, cubic sII, and hexagonal sH).[3] Given their abundance (NGHs have been identified as containing twice the energy stored in all other fossil fuel deposits),[2,4] NGHs can serve as potential unconventional energy sources in the future to compensate for the globally increasing demand for energy with increasing consumption. To date, depressurization and thermal stimulation have been proposed and verified as two efficient techniques for gas extraction from marine deposits.[1] However, gas production from hydrate resources involves geochemistry, geology, engineering thermophysics, and so forth. This results in significant challenges to accelerating the process of industrial production. Thus, knowledge of the kinetics of hydrate dissociation under various gas production conditions is the foundation for developing safe and efficient approaches for gas recovery from NGH reservoirs.

As early as the mid-1980s, dissociation experiments performed by Kim et al. showed that the dissociation rate of hydrates in the liquid phase was proportional to the hydrate surface area and the difference in the fugacity of methane under equilibrium pressure and dissociation pressure. In addition, a kinetic function was established to describe the hydrate dissociation process.[5] Subsequently, additional research studies have focused on hydrate dissociation behaviors via experimental and numerical simulation methods, and considerable achievements have been reported in understanding the hydrate phase-change process in different fields.[6−13] Limited by the spatial and temporal resolutions of the analysis methods, the mechanism of hydrate dissociation at the microscopic level remains to be determined. Molecular dynamics (MD) simulations, which are complementary to experimental observations, can intuitively show the static structure and dynamic behavior of molecules, discover new phenomena, clarify the essential mechanisms of dynamic processes, and provide new insights into the formation[14−22] and dissociation[23−28] behavior of hydrates. In MD simulations, the gas and water molecule separation process is described as a two-step pathway during the hydrate dissociation process:[23−25]

Received: July 16, 2022
Accepted: November 2, 2022
Published: November 15, 2022

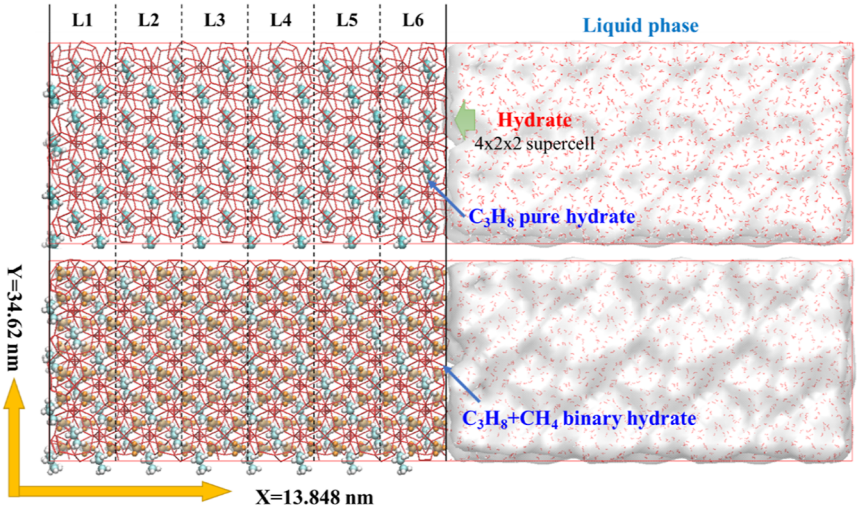

Figure 1. Initial configurations for the hydrate dissociation simulations, with pure propane hydrate shown in the top image and propane−methane binary hydrate shown in the bottom image. The hydrate clusters are divided into six parts along the *x*-axis, named L1−L6.

the hydrate cage formed by the H-bonded water network increases owing to the enhanced host diffusive behaviors, ultimately distorting and breaching the lattices, followed by the escape and diffusion of methane from the incomplete cages. The surface of the hydrate clusters shows a series of rapid decay and transition states, and the hydrates dissociate in a layer-by-layer manner.[23−28] On this basis, several studies have investigated the effects of temperature,[29,30] pressure,[26] salts,[31] static electrical fields,[32] and so forth on the dissociation process in the liquid phase using MD simulations. Recently, increasing attention has been paid to the hydrate dissociation process within a confined phase using a multi-phase initial system in MD simulations.[33−35] The results have shown that this dynamic behavior is quite different from that in the pure liquid phase, especially for the mass transfer of methane molecules.

However, most previous studies have focused on the dissociation process of sI hydrates (methane hydrate),[23−28,36−39] while less attention has been paid to sII and sH hydrates.[40−42] Although methane hydrate with an sI structure is the dominant structure in nature, sII and sH hydrates have been observed in several permafrost regions and marine sediments, such as the Gulf of Mexico, Cascadia Margin, and South China Sea.[43−45] In particular, in the Gulf of Mexico, sII hydrates account for more than 80% of the water in the near-seafloor core materials, as measured by carbon-13 nuclear magnetic resonance and powder X-ray diffraction (XRD) methods. In addition to permafrost regions and deep oceans, sII hydrates have been identified in gas/oil pipelines,[46] leading to extensive risk management in offshore operations. Therefore, understanding the behavior and evolution of sII hydrates is necessary and important not only for gas production from hydrate resources but also for flow assurance.

The unit cell of the sII hydrate structure is denoted as $16M_S8M_L136H_2O$, consisting of 8 large hexakaidecahedron cages ($5^{12}6^4$) and 16 small pentagonal dodecahedron cages (5^{12}).[47] Compared to the unit cell of the sI hydrate, the number of cages is greater in the sII hydrate unit cell and the volume for the large cages is increased, which indicates that larger guest molecules can be captured in sII hydrates. In reality, propane (C_3H_8) hydrates are one of the typical hydrates with sII crystalline structures, with C_3H_8 molecules are located only in the large cages owing to the size of the guest molecule. Additionally, the small cages of sII hydrates are often occupied by methane molecules with a relatively small size. These small molecules, which are called secondary "help-gases", serve to stabilize the crystal structure.[48−50] Therefore, both pure (C_3H_8) and binary (C_3H_8 + CH_4) hydrates in an sII structure are investigated, and the effects of host−host, guest−host, and guest−guest coupling interactions on the dissociation process of hydrates are also analyzed in this study.

2. SIMULATION METHOD

2.1. Initial Configuration. Based on previous studies of the dissociation behaviors of hydrates in sII structures in the liquid phase during heating, we established two initial multi-phase dissociation systems: the hydrate cluster and the liquid phase, as shown in Figure 1, in which the left moiety is the hydrate phase and the right is the pure liquid phase. These phases differ in that one is the pure C_3H_8 hydrate and the other is the C_3H_8 + CH_4 binary hydrate. Hydrates with sII structures were selected for investigation, and the construction of single-crystal cells can be divided into three processes.[51] (1) The positions of the oxygen atoms in the water molecule of the hydrate were determined by XRD. (2) By adjusting the orientation of hydrogen atoms in the water molecule to obey the Bernal−Fowler rule, the optimized configuration with the lowest potential energy and dipole moment of the unit cell was selected to determine the structure of the main water molecule. (3) The guest molecules were filled into the cages formed by the hydrogen-bonded network of water molecules. If only C_3H_8 molecules occupy the $5^{12}6^4$ large cages, which is called propane hydrate, the chemical formula is $8C_3H_8{\cdot}136H_2O$; when propane occupies the $5^{12}6^4$ large cages and methane occupies the 5^{12} small cages, which is called propane−methane binary hydrate, the chemical formula is $8C_3H_8{\cdot}16CH_4{\cdot}136H_2O$. Both hydrate lattice parameters are 1.731 nm (1 nm = 10 Å), and the space group is *Fd*3*m*.[52] The supercell of the hydrate phase in the initial system consists of 4 × 2 × 2 sII hydrate unit cells along the *x*−*y*−*z* directions, and the liquid phase consists of 2704 water molecules with a total system size of 13.848 × 3.462 × 3.462 nm. For the analysis, we divided the hydrate cluster into six equal layers (layers L1−L6) along the *x*-axis, as shown in Figure 1.

https://doi.org/10.1021/acsomega.2c04488
ACS Omega 2022, 7, 42774−42782

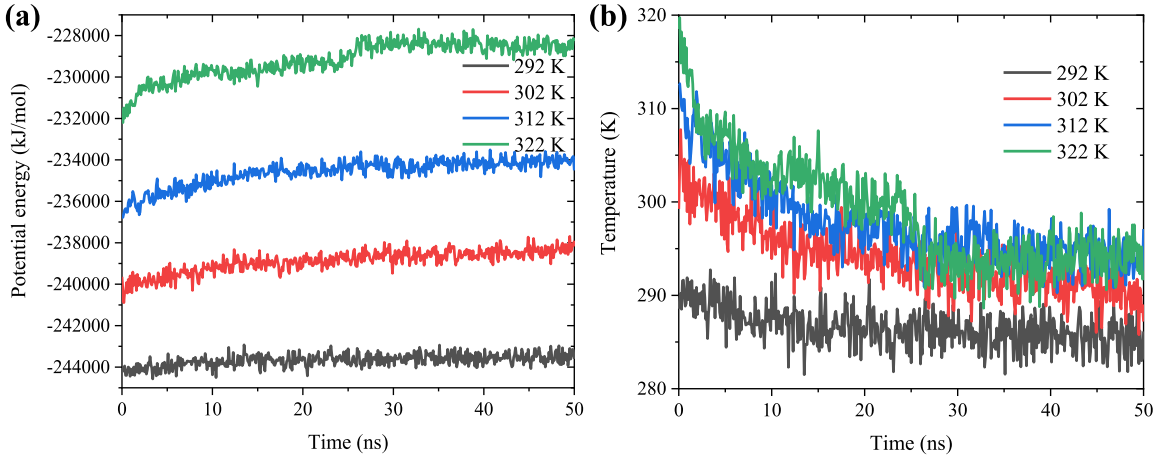

Figure 2. Time variation of the potential energy (a) and temperature (b) of the binary hydrate system at initial temperatures of 292, 302, 312, and 322 K.

2.2. Simulation Details. To obtain a more reasonable initial configuration, we utilized a conjugate gradient algorithm to minimize the energy of the system.[53] Then, short 200 ps *NVT* and *NPT* simulations were performed to equilibrate the temperature and pressure of the systems. The equilibrium temperatures were 292, 302, 312, and 322 K, and the equilibrium pressure was 3 MPa. Temperature coupling was implemented using velocity rescaling with a stochastic term,[54] and pressure control was realized using Parrinello−Rahman extended-ensemble pressure coupling.[55] A leap-frog algorithm was selected to integrate Newton's equation of motion with a 1 fs time step.[56] The thermostat constant was 0.1 ps, and the barostat constant was 1.0 ps. The final equilibrium configuration was selected as the initial configuration for the subsequent MD simulations, and the adiabatic *NVE* ensemble was used to investigate the hydrate dissociation process in the liquid phase. In the production simulations, the leap-frog algorithm was used for integrating Newton's equation of motion without pressure and temperature coupling.

The optimized potentials for liquid simulation all-atom (OPLS-AA) force field was used for the guest molecules (methane and propane);[57] the three-force point rigid SPC/E model was selected to describe the water molecules.[58] The particle grid Ewald method was used to calculate the long-range Coulomb interaction.[59] The van der Waals interactions were described using the Lennard−Jones potential with a cut-off distance of 1.2 nm, and periodic boundary conditions (PBCs) were applied for all simulations. To improve the accuracy, all the MD simulations were performed using the double-precision Gromacs software package (version 2018).[60,61]

2.3. Data Analysis. During the MD simulations, both the hydrate and liquid phases contain water and methane molecules. To distinguish the water molecules in the two phases, we used the F_3 order parameters proposed by Báez and Clancy to characterize the state of the water molecules.[23,62] In the solid phase, water molecules are arranged and oriented in a specific state, the nearest-neighbor water oxygen atoms of one water molecule can form a regular tetrahedron structure under ideal conditions, and the water oxygen atoms are located in the center of the regular tetrahedron structure. In contrast, in the liquid phase, the orientation of water molecules is random. Based on the F_3 order parameter, water molecules can be distinguished by the deviation of the state of the water oxygen atoms in the simulation system from the ideal standard tetrahedral structure.

$$F_{3,i} = \langle[\cos\theta_{jik}|\cos\theta_{jik}| + \cos^2 104.25]^2\rangle_{j,k}$$
$$= \{\sim 0.1 \text{ liquid water}$$
$$\sim 0.0 \text{ solid water (ice, hydrate)} \quad (1)$$

where θ_{jik} is the angle between water oxygen atom i and two adjacent water oxygen atoms. Water oxygen atoms j and k are located in the first water shell of the center oxygen atom (3.5 Å). When the average F_3 value approaches 0.1, the water molecules are close to the liquid state, and when the average F_3 order parameter is equal to zero, the water molecules are in the solid state, including ice and hydrates.

3. RESULTS AND DISCUSSION

3.1. Effects of the Initial Temperature on sII Hydrate Dissociation in the Liquid Phase. Hydrate dissociation is the phase change process from a solid to a liquid phase. With hydrate dissociation, the arrangement of host water molecules gradually changes from a space lattice to a random disordered state, and guest molecules are released into the liquid phase. The rearrangement of the spatial structure leads to an increase in the potential energy of the system, as shown in Figure 2a. Because an adiabatic ensemble (*NVE*) is used, there is no mass or heat transfer between the simulation system and the outside environment. Therefore, the increase in potential energy must be supplied by the kinetic energy of the system during hydrate dissociation, resulting in a decrease in the system temperature, as shown in Figure 2b.

Although the system temperatures gradually decrease with different initial temperatures, the degree of reduction varies. A maximum temperature drop of approximately 25 K is obtained for the simulation with an initial temperature of 322 K. For the simulation with an initial temperature of 292 K, the variations in the potential energy and temperature of the system are very different: the temperature of the system decreases within the first 10 ns, and the system temperature becomes constant with a fluctuating equilibrium state. This result indicates that the hydrate dissociation behavior can be stopped under a low initial temperature condition, which is also consistent with the actual mining process.

https://doi.org/10.1021/acsomega.2c04488
ACS Omega 2022, 7, 42774−42782

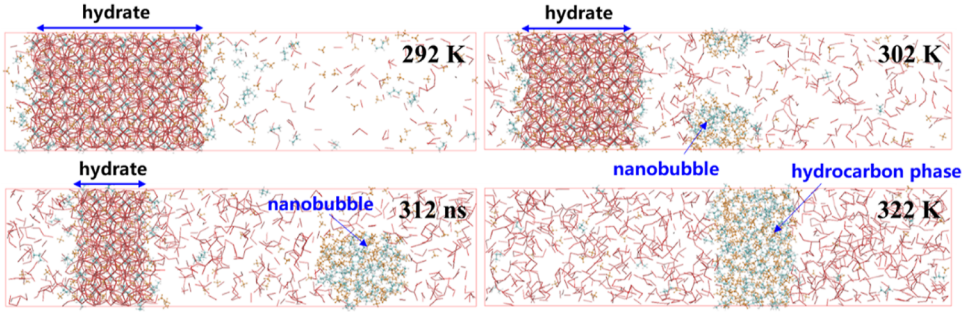

Figure 3. Final snapshots after 50 ns MD simulations at different initial temperatures; residual hydrate clusters and gas clusters are presented.

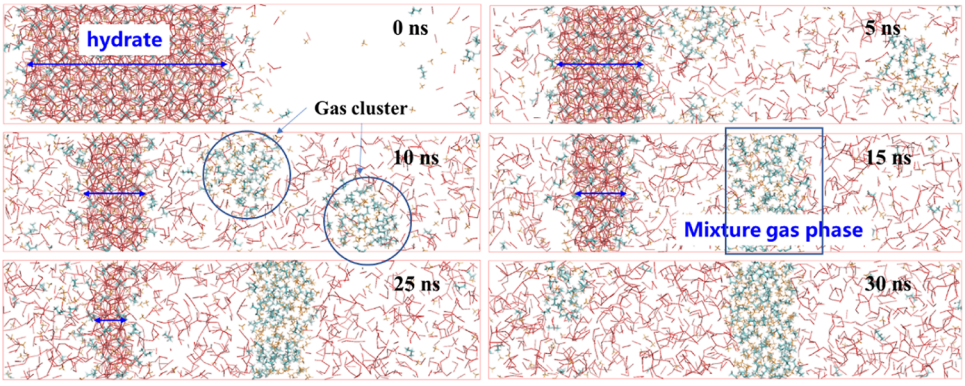

Figure 4. Six snapshots in the *xy* plane of the binary sII hydrate at different dissociation times (initial temperature T = 322 K); gas clusters and the mixed hydrocarbon phase are marked.

In Figure 3, final snapshots of the MD simulations under four different initial temperature conditions are shown. The results indicate that the hydrate dissociation rate is sensitive to the initial temperature of the system: at an initial temperature of 322 K, the hydrate completely dissociates during the MD simulation time; in contrast, residual hydrate clusters remain in the liquid after 50 ns MD simulations with the other initial system conditions. Overall, the higher the initial temperature is, the less residual hydrate there will be. The system temperature can be decreased during the hydrate dissociation process, and the dissociation behavior can be stopped when the temperature decreases below the phase equilibrium temperature. The hydrate clusters hardly dissociate at an initial temperature of 292 K. Therefore, in the practice of gas extraction from hydrate reservoirs, the temperature decrease caused by the endothermic hydrate dissociation process cannot be ignored. Depressurization is the most effective method for extracting natural gas from hydrates. When the heat consumption in the hydrate dissociation process cannot be replenished by the latent heat of sediments, the hydrate dissociation rate slows, and the pressure−temperature conditions return to the region of hydrate phase equilibrium, leading to the cessation of the dissociation behavior and hydrate secondary formation. Therefore, a sufficient heat supply is necessary to maintain hydrate dissociation at a constant rate with high efficiency. In addition, we believe that using the *NVE* ensemble provides the closest approximation of the actual situation for studying the dissociation behavior of hydrates, and the results of our simulations with the *NVE* ensemble are reasonable.

3.2. Kinetics of sII Hydrate Dissociation in the Liquid Phase. Using the initial configuration and parameter settings described in the previous section and taking the dissociation process of C_3H_8 + CH_4 binary hydrate at an initial temperature of 322 K as an example, Figure 4 shows six *xy* time-lapse snapshots of the hydrate dissociation at different simulation times. Because the temperature of the system is higher than the hydrate phase equilibrium temperature, hydrate phase transition occurs. The blue bidirectional arrows indicate the residual hydrate; in general, over time, the hydrate cluster dissociates in a layer-by-layer manner (due to the PBCs, the hydrate decomposes from both the left and right sides toward the central region of the hydrate simultaneously). Dissociation preferentially occurs on the hydrate cluster surface until the dissociation behavior is completed, and the hydrate phase dissociation front is almost a plane owing to the PBCs. As the hydrate decomposes, the guest molecules encapsulated in the hydrate cage are released and diffuse into the liquid phase. A large number of guest molecules gradually spread into the liquid phase with hydrate dissociation. Owing to the low solubility of methane and propane molecules in the liquid phase, the liquid phase rapidly becomes oversaturated, and nanobubbles and hydrocarbon phases form. As shown in Figure 4, several gas clusters appear in the system at the early dissociation stage (0−10 ns); a cubic region of hydrocarbon phase then forms in the liquid phase owing to the PBCs, and this region contains mixed methane and propane molecules. The formation of nanobubbles and hydrocarbon phase can increase the chemical potential difference between the hydrate and liquid phases, thus accelerating hydrate dissociation.[63,64] However, in a confined space, if nanobubbles cannot spread out in time during hydrate dissociation, it is possible for a rapid increase in pressure to occur in the pore, which has a negative impact on further dissociation of hydrates. The general sII hydrate dissociation mechanism is shown in Figure 4, and it is almost consistent with the sI hydrate mechanism.[24−29]

https://doi.org/10.1021/acsomega.2c04488
ACS Omega 2022, 7, 42774−42782

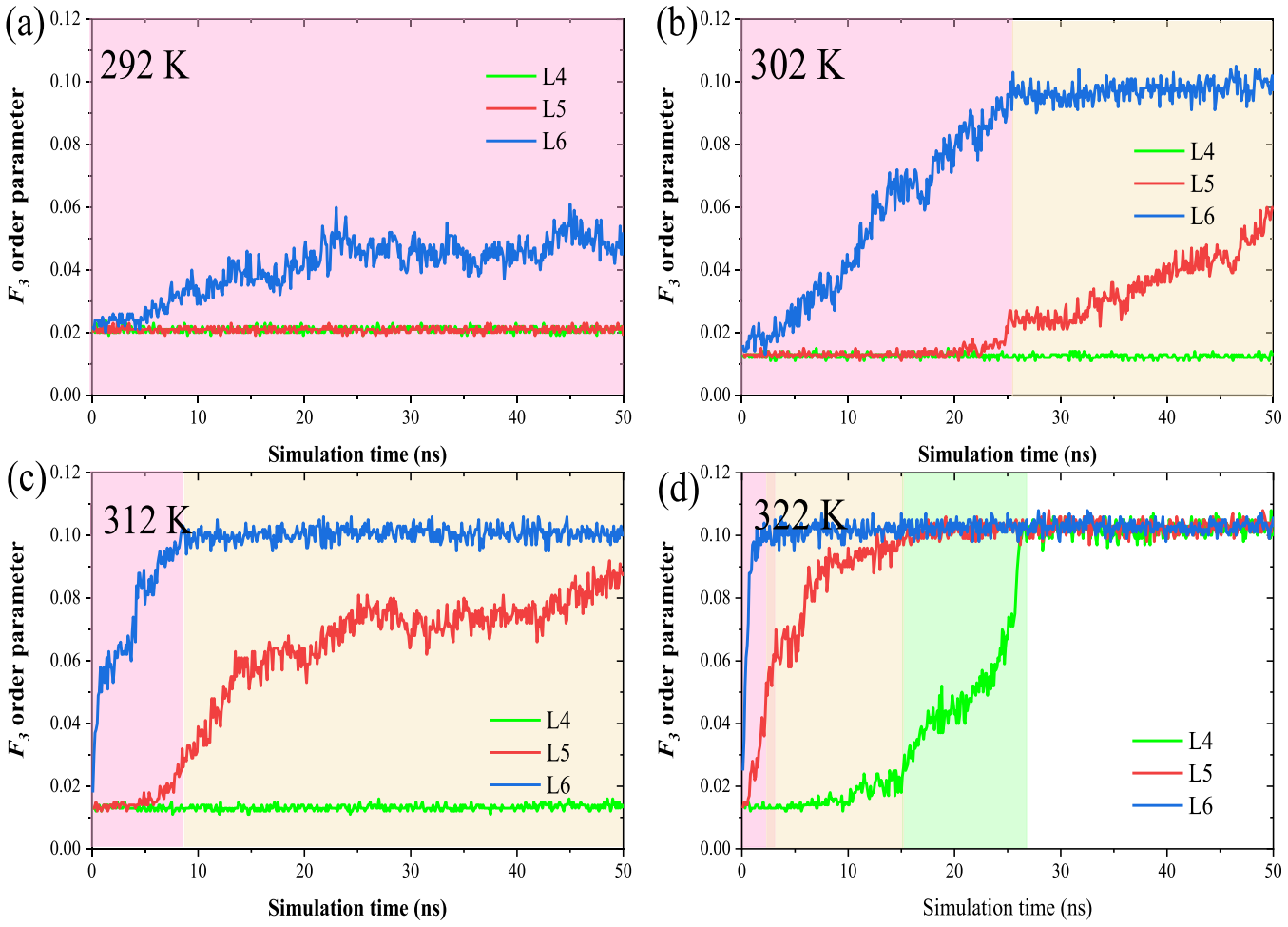

Figure 5. Time variation of the average F_3 order parameters for each layer at different initial temperatures of 292 (a), 302 (b), 312 (c), and 322 K (d).

To quantify the dissociation process of the sII hydrates, the hydrate cluster is divided into six equally spaced layers (L1−L6), as shown in Figure 1. Because PBCs are used in our simulations, the time variation of the hydrate cluster is almost symmetrical; therefore, we only present the time variation of the average F_3 order parameter for layers L4−L6 under different initial dissociation temperature conditions in Figure 5 (L4 is the inner layer and L6 is the outermost layer facing the liquid phase in the initial simulation configuration). It should be noted that the average F_3 order parameters for the L6 hydrate layer initially increase to 0.1 (liquid phase); subsequently, the average F_3 order parameters for layer L5 increase, and finally, the average F_3 order parameters for layer L4 increase. This result is independent of the initial simulation temperature. Because the hydrate phase has already decomposed during the equilibrium simulations, the initial value of the average F_3 for the L6 hydrate layer may be larger than those for the other layers. These results directly confirm that hydrate dissociation in the liquid phase is a phase transition process from the outer layer to the inner layer. Moreover, the inner layer of the hydrate does not decompose until the outer layer is completely broken down, which indicates that the presence of the outer layer of the hydrate can prevent decomposition of the inner hydrate layer.

Although the dissociation pathways of the sII hydrate phase are almost the same, the dissociation time for each hydrate layer differs under different initial temperature conditions. When the initial dissociation temperature is 292 K (Figure 5a), only the values of F_3 for the L6 layer increase, and the maximum equilibrium value does not increase to 0.1. This indicates that the outermost layer of the hydrate does not decompose during the simulation time at this initial temperature, and the inner layer remains in the hydrate phase. When the initial temperature increases to 302 K (Figure 5b), the outermost L6 hydrate layer is dissociated at ∼25 ns. After the L6 layer is dissociated, the hydrate cluster in layer L5 begins to decompose, and this layer does not break down fully at the end of the MD simulation. When the initial temperature increases further to 312 K (Figure 5c), the outermost hydrate layer is broken down completely at ∼9 ns, and the dissociation of the hydrate in layer L5 does not finish by the end of the simulation; however, more of the hydrate in layer L5 dissociates than at an initial dissociation temperature of 302 K. When the initial temperature is 322 K (Figure 5d), the outermost layer is dissociated at 3 ns, the hydrate in layer L5 layer is dissociated within 15 ns, and the hydrate in the inner layer L4 becomes a liquid phase at 27 ns. According to the F_3 curves for the three layers, the dissociation time for the inner hydrate layer is longer than that for the outer layer because of the temperature drops during the dissociation process. It should be noted that the value of F_3 for layer L4 increases rapidly in the final stage of hydrate dissociation (26−27 ns)

https://doi.org/10.1021/acsomega.2c04488
ACS Omega 2022, 7, 42774−42782

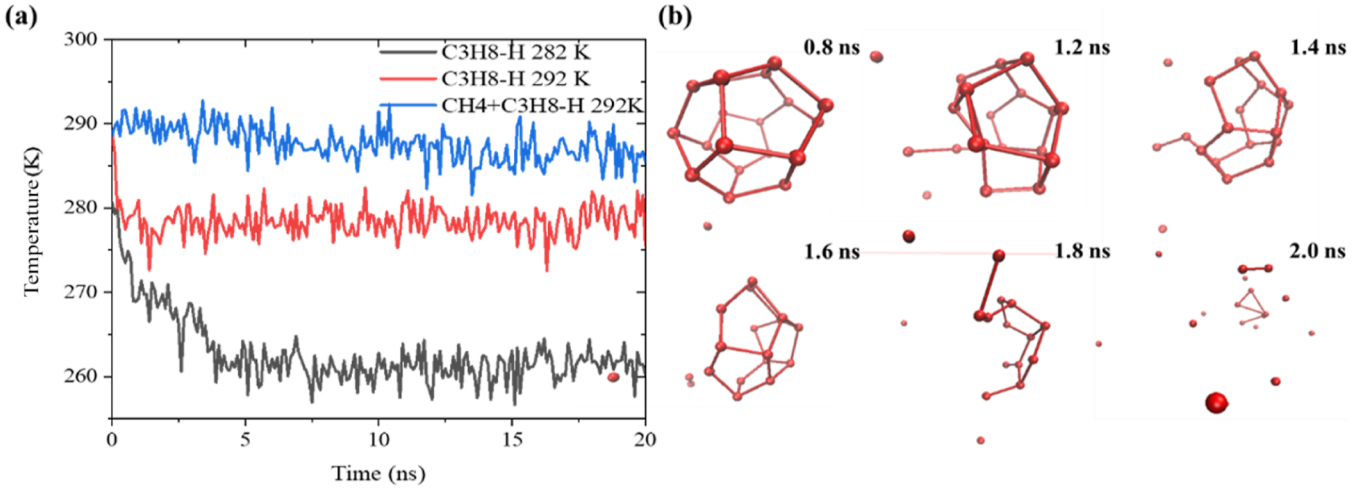

Figure 6. (a) Time variation of the system temperature for the pure and binary hydrate systems under different initial temperature conditions; (b) snapshots of the small cage dissociation process in pure propane hydrate.

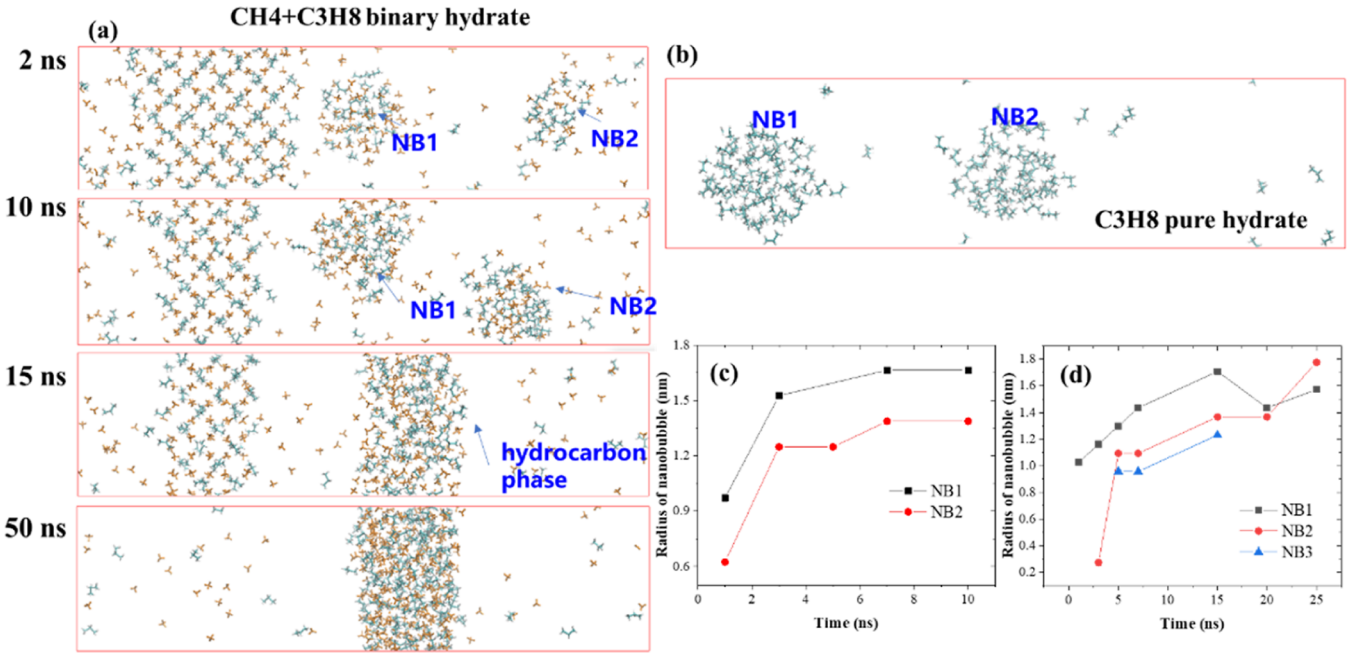

Figure 7. Snapshots showing the evolution of nanobubbles/hydrocarbon phase (a) and time variation of nanobubble sizes (c) in a binary sII hydrate dissociation system at an initial temperature of 322 K; (b) snapshot showing the final state (b) and time variation of nanobubble sizes (d) for the pure propane hydrate system at an initial temperature of 282 K. Water molecules are not shown. Due to the difference in guest molecule density, the boundary between water and hydrocarbon phase can be distinguished easily. Nanobubble is abbreviated as NB in this figure.

under an initial temperature of 322 K because the guest molecules are released from the cages and the residual hydrate cages collapse easily without the support of guest molecules during this stage.

3.3. Effect of Guest Molecule Occupancy on the Dissociation Behavior. Both pure propane hydrate and methane + propane binary hydrate crystals are sII hydrate structures. Figure 6a presents the time variation of the system temperature for the two hydrate systems under the same initial temperature (292 K). Under this initial temperature condition, the binary hydrate temperature decreases slowly in the primary stage and reaches a dynamic equilibrium, as discussed above. In contrast, the system temperature of pure propane hydrate decreases rapidly (~13 K) within 2 ns, which indicates that the pure propane hydrate quickly transforms to a liquid phase, while most of the methane + propane binary hydrate cluster remains in the solid state. When the initial system temperature is decreased to 282 K, the MD simulation results in the *NVE* ensemble show that the dissociation time increases to 5 ns for the pure propane hydrate, and the temperature drops by approximately 22 K. Based on the simulation results, pure propane sII hydrates decompose faster than binary hydrates under the same initial temperature and pressure conditions, which is mainly attributed to the occupation of methane molecules in the small cages of binary propane hydrates. The occupation of guest molecules stabilizes the crystal cage and decreases the hydrate dissociation rate.[65,66]

Figure 6b shows the dissociation process of the small cage without guest molecules; the empty cage collapses quickly. Compared to the small cage with guest occupation, only one

https://doi.org/10.1021/acsomega.2c04488
ACS Omega 2022, 7, 42774−42782

step occurs in the collapse of the empty cage: the collapse begins on one side of the cage and spreads to the entire cage, unlike the two-step pathway induced by the guest−host interaction. For the cage with a guest molecule, the dissociation process begins on one cage side; the enhanced diffusion of water molecules on one cage side leads to breaking of the water cage. Subsequently, the guest molecule diffuses from this incomplete cage; snapshots are shown in Figure S2; this dynamics process is similar to the previous results.[23−25] The diffusion of guest molecules from an incomplete cage takes a certain amount of time, and unreleased guest molecules within the hydrate cages continue to stabilize the cages at this time. Finally, the cage dissociation rate increases rapidly after the guest molecule escapes from the incomplete cage. The presence of guest molecules in small cages is the reason that the pure propane hydrate dissociates faster than the propane + methane binary hydrate.

3.4. Evolution of Gas Clusters. The goal of hydrate exploration and exploitation is to extract natural gas from hydrate resources; therefore, the mass transfer of guest molecules is the focus of our attention. As shown in Figure 4, guest molecules (both methane and propane) are released from the hydrate cage and diffuse into the liquid phase. These molecules then aggregate into a small gas cluster owing to the low solubility of small hydrocarbon molecules in water, and these clusters eventually evolve into nanobubbles (Figures 4 and 7). Previous studies have demonstrated that nanobubbles are the main form of released gas molecules and also play an essential role in the further dissociation of residual hydrate,[63,64] especially in confined pore spaces.[33−35]

In Figure 7a, the evolution of gas clusters in the propane + methane binary hydrate system at the 322 K initial temperature condition is shown intuitively, and the variation in nanobubble sizes with time is shown in Figure 7c. Because of the PBCs, both hydrate surfaces are preferentially dissociated, leading to the formation of two nanobubbles near the two dissociation fronts at 1 ns; methane and propane molecules are mixed in the nanobubbles. As the hydrate dissociation proceeds, more methane and propane molecules are released from the dissociation front surfaces; the two nanobubbles grow in cylindrical shapes owing to the PBC in the *z*-direction, and eventually, the two nanobubbles merge and evolve into a hydrocarbon phase at 10 ns. Compared to the binary hydrate, in the pure hydrate, three propane nanobubbles were formed within 5 ns due to the propane releasing from the hydrate cluster at an initial temperature of 282 K (Figure 7d). Nanobubbles gradually grew, and two of these merged into each other to finally form a larger one at 15 ns. Thereby, two nanobubbles exist in the liquid phase and do not form the hydrocarbon phase before the simulation is finished (Figure 7b). This phenomenon is induced by the number of guest molecules; there are eight propane molecules and 16 methane molecules in the binary unit sII hydrate, whereas there are only eight propane molecules in the pure sII hydrate.

4. CONCLUSIONS

MD simulations were used to investigate the dissociation processes of pure and binary sII hydrates in the liquid phase under a series of initial temperature conditions in an adiabatic ensemble (*NVE*). Through the simulations, we clarified the relationship between sII hydrate dissociation behavior and temperature as well as the difference in sII dissociation behavior between pure and binary hydrates. The simulation results showed that the higher the initial temperature, the faster the rate of hydrate dissociation would be, and this trend was independent of the structure and guest occupancy of the hydrate. Because hydrate dissociation is an endothermic process, the temperature of the system drops during the dissociation process, which slows the further dissociation of the residual hydrate. Under the initial temperature conditions in the simulations, both pure and binary sII hydrates dissociated from the outside to inside, similar to the behavior of the sI hydrate, and the inner layer of the hydrate could break down only after all of the outer layers of the hydrate had dissociated. At the same dissociation temperature, the dissociation rate of pure propane hydrate was much faster than that of binary hydrates because the empty small cages collapsed more easily without support from guest molecules. In addition, guest gas molecules were released from the hydrate phase and rapidly evolved into nanobubbles. In the binary hydrate system, these nanobubbles merged and formed a hydrocarbon phase owing to the large number of gas molecules.

This study revealed the microscopic dissociation dynamics of pure and binary sII hydrates. The simulation results can provide an understanding of the effects of the hydrate crystal structure and guest occupancy on the hydrate dissociation behavior, which is the theoretical basis for hydrate exploitation with high efficiency.

■ ASSOCIATED CONTENT

Supporting Information

The Supporting Information is available free of charge at https://pubs.acs.org/doi/10.1021/acsomega.2c04488.

> Initial configurations of the hydrate dissociation for the MD production simulations at the initial temperatures of 282 and 292 K and snapshots of the dissociation process of the small cage with a guest molecule (methane) in the propane + methane binary hydrate (PDF)

■ AUTHOR INFORMATION

Corresponding Author

Bin Fang − *School of Mathematics and Physics, China University of Geosciences, Wuhan 430074, China; Process and Energy Department, Delft University of Technology, 2628CB Delft, The Netherlands;* orcid.org/0000-0003-0909-2151; Email: fangbin126@cug.edu.cn

Authors

Peihan Yang − *School of Mathematics and Physics, China University of Geosciences, Wuhan 430074, China*

Dongdong Guo − *School of Earth and Environment, Anhui University of Science & Technology, Huainan 232001, China*

Complete contact information is available at: https://pubs.acs.org/10.1021/acsomega.2c04488

Notes

The authors declare no competing financial interest.

■ ACKNOWLEDGMENTS

This work was supported by the National Natural Science Foundation of China (no. 42206235) and the International Postdoctoral Exchange Fellowship Program (no. PC2021073).

REFERENCES

(1) Sloan, E. D., Jr.; Koh, C. A.*Clathrate Hydrates of Natural Gases*; CRC Press, 2007.
(2) Li, X. S.; Xu, C. G.; Zhang, Y.; Ruan, X. K.; Li, G.; Wang, Y. Investigation into gas production from natural gas hydrate: A review. *Appl. Energy* **2016**, *172*, 286−322.
(3) Ripmeester, J. A.; Tse, J. S.; Ratcliffe, C. I.; Powell, B. M. A New Clathrate Hydrate Structure. *Nature* **1987**, *325*, 135−136.
(4) Florusse, L. J.; Peters, C. J.; Schoonman, J.; Hester, K. C.; Koh, C. A.; Dec, S. F.; Marsh, K. N.; Sloan, E. D. Stable low-pressure hydrogen clusters stored in a binary clathrate hydrate. *Science* **2004**, *306*, 469−471.
(5) Kim, H. C.; Bishnoi, P. R.; Heidemann, R. A.; Rizvi, S. S. H. Kinetics of methane hydrate decomposition. *Chem. Eng. Sci.* **1987**, *42*, 1645−1653.
(6) Yang, X.; Sun, C.-Y.; Yuan, Q.; Ma, P.-C.; Chen, G.-J. Experimental Study on Gas Production from Methane Hydrate-Bearing Sand by Hot-Water Cyclic Injection. *Energy Fuels* **2010**, *24*, 5912−5920.
(7) Zhang, Z.; Li, C.; Ning, F.; Liu, L.; Cai, J.; Liu, C.; Wu, N.; Wang, D. Pore Fractal Characteristics of Hydrate-bearing Sands and Implications to the Saturated Water Permeability. *J. Geophys. Res.: Solid Earth* **2020**, *125*, No. e2019JB018721.
(8) Li, C.; Liu, C.; Hu, G.; Sun, J.; Hao, X.; Liu, L.; Meng, Q. Investigation on the multiparameter of hydrate-bearing sands using nano-focus X-ray compsuted tomography. *J. Geophys. Res.: Solid Earth* **2019**, *124*, 2286−2296.
(9) Ta, X. H.; Yun, T. S.; Muhunthan, B.; Kwon, T. H. Observations of pore-scale growth patterns of carbon dioxide hydrate using X-ray computed microtomography. *Geochem., Geophys., Geosyst.* **2015**, *16*, 912−924.
(10) Lei, L.; Seol, Y.; Choi, J. H.; Kneafsey, T. Pore habit of methane hydrate and its evolution in sediment matrix—Laboratory visualization with phase-contrast micro-CT. *Mar. Pet. Geol.* **2019**, *104*, 451−467.
(11) Kuang, Y.; Zhang, L.; Song, Y.; Yang, L.; Zhao, J. Quantitative determination of pore-structure change and permeability estimation under hydrate phase transition by NMR. *AIChE J.* **2020**, *66*, 16859.
(12) Ji, Y.; Hou, J.; Liu, Y.; Du, Q.Study on Formation and Dissociation of Methane Hydrate in Sandstone Using Low-Field Nuclear Magnetic Resonance Technology. *39th International Conference on Ocean, Offshore and Arctic Engineering*, 2020.
(13) Ge, X.; Liu, J.; Fan, Y.; Xing, D.; Deng, S.; Cai, J. Laboratory Investigation Into the Formation and Dissociation Process of Gas Hydrate by Low-Field NMR Technique. *J. Geophys. Res.: Solid Earth* **2018**, *123*, 3339−3346.
(14) Sloan, E. D., Jr. Fundamental principles and applications of natural gas hydrates. *Nature* **2003**, *426*, 353−359.
(15) Sloan, E.; Fleyfel, F. A molecular mechanism for gas hydrate nucleation from ice. *AlChE J* **1991**, *37*, 1281−1292.
(16) Long, J.Gas Hydrate Formation Mechanism and Kinetic Inhibition. Ph.D. Thesis, Colerado School of Mines, 1994.
(17) Radhakrishnan, R.; Trout, B. L. A new approach for studying nucleation phenomena using molecular simulations: Application to CO 2 hydrate clathrates. *J. Chem. Phys.* **2002**, *117*, 1786−1796.
(18) Jacobson, L. C.; Hujo, W.; Molinero, V. Amorphous Precursors in the Nucleation of Clathrate Hydrates. *J. Am. Chem. Soc.* **2010**, *132*, 11806−11811.
(19) He, Z.; Linga, P.; Jiang, J. What are the key factors governing the nucleation of CO2 hydrate? *Phys. Chem. Chem. Phys.* **2017**, *19*, 15657−15661.
(20) Zhang, Z.; Walsh, M. R.; Guo, G.-J. Microcanonical molecular simulations of methane hydrate nucleation and growth: Evidence that direct nucleation to sI hydrate is among the multiple nucleation pathways. *Phys. Chem. Chem. Phys.* **2015**, *17*, 8870−8876.
(21) Bi, Y.; Porras, A.; Li, T. Free energy landscape and molecular pathways of gas hydrate nucleation. *J. Chem. Phys.* **2016**, *145*, 211909.
(22) Li, L.; Zhong, J.; Yan, Y.; Zhang, J.; Xu, J.; Francisco, J. S.; Zeng, X. C. Unraveling nucleation pathway in methane clathrate formation. *Proc. Natl. Acad. Sci.* **2020**, *117*, 24701−24708.
(23) Báez, L. A.; Clancy, P. Computer-Simulation of the Crystal-Growth and Dissolution of Natural-Gas Hydrates. *Ann. N. Y. Acad. Sci.* **1994**, *715*, 177−186.
(24) Reshadi, P.; Modarress, H.; Dabir, B.; Amjad-Iranagh, S. A study on dissociation of sII krypton hydrate and the effect of hydrocarbon guest molecules as stabilizer by molecular dynamics simulation. *Phase Transitions* **2017**, *90*, 1128−1142.
(25) Liu, Y.; Zhao, J. J.; Xu, J. C. Dissociation mechanism of carbon dioxide hydrate by molecular dynamic simulation and ab initio calculation. *Comput. Theor. Chem.* **2012**, *991*, 165−173.
(26) Yan, K. F.; Li, X. S.; Chen, Z. Y.; Li, B.; Xu, C. G. Molecular dynamics simulation of methane hydrate dissociation by depressurisation. *Mol. Simul.* **2013**, *39*, 251−260.
(27) Bagherzadeh, S. A.; Englezos, P.; Alavi, S.; Ripmeester, J. A. Molecular Modeling of the Dissociation of Methane Hydrate in Contact with a Silica Surface. *J. Phys. Chem. B* **2012**, *116*, 3188−3197.
(28) English, N. J.; Johnson, J. K.; Taylor, C. E. Molecular-dynamics simulations of methane hydrate dissociation. *J. Chem. Phys.* **2005**, *123*, 244503.
(29) Bagherzadeh, S. A.; Alavi, S.; Ripmeester, J.; Englezos, P. Formation of methane nano-bubbles during hydrate decomposition and their effect on hydrate growth. *J. Chem. Phys.* **2015**, *142*, 214701.
(30) Iwai, Y.; Nakamura, H.; Arai, Y.; Shimoyama, Y. Analysis of dissociation process for gas hydrates by molecular dynamics simulation. *Mol. Simul.* **2010**, *36*, 246−253.
(31) Yagasaki, T.; Matsumoto, M.; Andoh, Y.; Okazaki, S.; Tanaka, H. Dissociation of Methane Hydrate in Aqueous NaCl Solutions. *J. Phys. Chem. B* **2014**, *118*, 11797−11804.
(32) Chen, J.; Liu, C.; Zhang, Z.; Wu, N.; Liu, C.; Ning, F.; Fang, B.; Wan, Y.; Bu, Q.; Hu, G. Molecular study on the behavior of methane hydrate decomposition induced by ions electrophoresis. *Fuel* **2022**, *307*, 121866.
(33) Fang, B.; Lü, T.; Ning, F.; Pang, J.; He, Z.; Sun, J. Facilitating gas hydrate dissociation kinetics and gas migration in clay interlayer by surface cations shielding effects. *Fuel* **2022**, *318*, 123576.
(34) Fang, B.; Ning, F.; Ou, W.; Wang, D.; Zhang, Z.; Yu, Y.; Lu, H.; Wu, J.; Vlugt, T. J. H. The dynamic behavior of gas hydrate dissociation by heating in tight sandy reservoirs: A molecular dynamics simulation study. *Fuel* **2019**, *258*, 116106.
(35) Fang, B.; Lü, T.; Cheng, L.; Wang, D.; Ni, Y.; Fan, B.; Meng, J.; Vlugt, T. J. H.; Ning, F. Negative Effects of Inorganic Salt Invasion on the Dissociation Kinetics of Silica-Confined Gas Hydrate via Thermal Stimulation. *Energy Fuels* **2022**, *36*, 6216−6228.
(36) Ning, F. L.; Glavatskiy, K.; Ji, Z.; Kjelstrup, S.; Vlugt, T. J. H. Compressibility, thermal expansion coefficient and heat capacity of CH4 and CO2 hydrate mixtures using molecular dynamics simulations. *Phys. Chem. Chem. Phys.* **2015**, *17*, 2869−2883.
(37) Jendi, Z. M.; Servio, P.; Rey, A. D. Ab initio modelling of methane hydrate thermophysical properties. *Phys. Chem. Chem. Phys.* **2016**, *18*, 10320−10328.
(38) Costandy, J.; Michalis, V. K.; Tsimpanogiannis, I. N.; Stubos, A. K.; Economou, I. G. Lattice constants of pure methane and carbon dioxide hydrates at low temperatures. Implementing quantum corrections to classical molecular dynamics studies. *J. Chem. Phys.* **2016**, *144*, 124512.
(39) Costandy, J.; Michalis, V. K.; Tsimpanogiannis, I. N.; Stubos, A. K.; Economou, I. G. Molecular dynamics simulations of pure methane and carbon dioxide hydrates: lattice constants and derivative properties. *Mol. Phys.* **2016**, *114*, 2672−2687.
(40) Erfan-Niya, H.; Modarress, H.; Zaminpayma, E. Computational study on the structure II clathrate hydrate of methane and large guest molecules. *J. Inclusion Phenom. Macrocyclic Chem.* **2011**, *70*, 227−239.
(41) Vlasic, T. M.; Servio, P.; Rey, A. D. Atomistic modeling of structure II gas hydrate mechanics: Compressibility and equations of state. *AIP Adv.* **2016**, *6*, 085317.

https://doi.org/10.1021/acsomega.2c04488
ACS Omega 2022, 7, 42774−42782

(42) Fang, B.; Ning, F.; Cao, P.; Peng, L.; Wu, J.; Zhang, Z.; Vlugt, T. J. H.; Kjelstrup, S. Modeling Thermodynamic Properties of Propane or Tetrahydrofuran Mixed with Carbon Dioxide or Methane in Structure-II Clathrate Hydrates. *J. Phys. Chem. C* **2017**, *121*, 23911−23925.
(43) Seol, J.; Lee, H. Natural gas hydrate as a potential energy resource: From occurrence to production. *Korean J. Chem. Eng.* **2013**, *30*, 771−786.
(44) Brooks, J. M.; Kennicutt, M. C.; Fay, R. R.; McDonald, T. J.; Sassen, R. Thermogenic Gas Hydrates in the Gulf of Mexico. *Science* **1984**, *225*, 409−411.
(45) Davidson, D. W.; Garg, S. K.; Gough, S. R.; Handa, Y. P.; Ratcliffe, C. I.; Ripmeester, J. A.; Tse, J. S.; Lawson, W. F. Laboratory Analysis of a Naturally-Occurring Gas Hydrate from Sediment of the Gulf of Mexico. *Geochim. Cosmochim. Acta* **1986**, *50*, 619−623.
(46) Fang, B.; Ning, F.; Hu, S.; Guo, D.; Ou, W.; Wang, C.; Wen, J.; Sun, J.; Liu, Z.; Koh, C. A. The effect of surfactants on hydrate particle agglomeration in liquid hydrocarbon continuous systems: a molecular dynamics simulation study. *RSC Adv.* **2020**, *10*, 31027−31038.
(47) Mak, T. C. W.; McMullan, R. K. Polyhedral Clathrate Hydrates. X. Structure of the Double Hydrate of Tetrahydrofuran and Hydrogen Sulfide. *J. Chem. Phys.* **1965**, *42*, 2732−2737.
(48) Larionov, E. G.; Manakov, A. Y.; Zhurko, F. V.; Dyadin, Y. A. CS-II binary clathrate hydrates at pressures of up to 15 kbar. *J. Struct. Chem.* **2000**, *41*, 476−482.
(49) Ripmeester, J. A.; Ratcliffe, C. I. Xe-129 Nmr-Studies of Clathrate Hydrates - New Guests for Structure-Ii and Structure-H. *J. Phys. Chem.* **1990**, *94*, 8773−8776.
(50) Alavi, S.; Ripmeester, J. A. Effect of small cage guests on hydrogen bonding of tetrahydrofuran in binary structure II clathrate hydrates. *J. Chem. Phys.* **2012**, *137*, 054712.
(51) Takeuchi, F.; Hiratsuka, M.; Ohmura, R.; Alavi, S.; Sum, A. K.; Yasuoka, K. Water proton configurations in structures I, II, and H clathrate hydrate unit cells. *J. Chem. Phys.* **2013**, *138*, 124504.
(52) Gabitto, J. F.; Tsouris, C. Physical properties of gas hydrates: A review. *J. Thermodyn.* **2010**, *2010*, 271291.
(53) Zimmermann, K. ORAL: All purpose molecular mechanics simulator and energy minimizer. *J. Comput. Chem.* **1991**, *12*, 310−319.
(54) Bussi, G.; Donadio, D.; Parrinello, M. Canonical sampling through velocity rescaling. *J. Chem. Phys.* **2007**, *126*, 014101.
(55) Parrinello, M.; Rahman, A. Polymorphic transitions in single crystals: A new molecular dynamics method. *J. Appl. Phys.* **1981**, *52*, 7182−7190.
(56) Frenkel, D.; Smit, B.; Ratner, M. A. Understanding molecular simulation: From algorithms to applications. *Phys. Today* **1997**, *50*, 66.
(57) Martin, M. G.; Siepmann, J. I. Transferable potentials for phase equilibria. 1. United-atom description of n-alkanes. *J. Phys. Chem. B* **1998**, *102*, 2569−2577.
(58) Berendsen, H. J. C.; Grigera, J. R.; Straatsma, T. P. The missing term in effective pair potentials. *J. Chem. Phys.* **1987**, *91*, 6269−6271.
(59) Essmann, U.; Perera, L.; Berkowitz, M. L.; Darden, T.; Lee, H.; Pedersen, L. G. A Smooth Particle Mesh Ewald Method. *J. Chem. Phys.* **1995**, *103*, 8577−8593.
(60) Hess, B.; Kutzner, C.; van der Spoel, D.; Lindahl, E. GROMACS 4: Algorithms for highly efficient, load-balanced, and scalable molecular simulation. *J. Chem. Theory Comput.* **2008**, *4*, 435−447.
(61) Abraham, M. J.; Murtola, T.; Schulz, R.; Páll, S.; Smith, J. C.; Hess, B.; Lindahl, E. J. S. GROMACS: High performance molecular simulations through multi-level parallelism from laptops to supercomputers. *SoftwareX* **2015**, *1−2*, 19−25.
(62) Uttormark, M. J.; Thompson, M. O.; Báez, L. A.; Clancy, P. Solid-Liquid Cluster Recognition in Heterogeneous Systems. *Mol. Simul.* **1993**, *11*, 121−144.
(63) Yagasaki, T.; Matsumoto, M.; Andoh, Y.; Okazaki, S.; Tanaka, H. Dissociation of methane hydrate in aqueous NaCl solutions. *J. Phys. Chem. B* **2014**, *118*, 11797−11804.
(64) Yagasaki, T.; Matsumoto, M.; Tanaka, H. Effects of thermodynamic inhibitors on the dissociation of methane hydrate: a molecular dynamics study. *Phys. Chem. Chem. Phys.* **2015**, *17*, 32347−32357.
(65) Myshakin, E. M.; Jiang, H.; Warzinski, R. P.; Jordan, K. D. Molecular Dynamics Simulations of Methane Hydrate Decomposition. *J. Phys. Chem. A* **2009**, *113*, 1913−1921.
(66) Windmeier, C.; Oellrich, L. R. Theoretical Study of Gas Hydrate Decomposition Kinetics-Model Development. *J. Phys. Chem. A* **2013**, *117*, 10151−10161.

https://doi.org/10.1021/acsomega.2c04488
ACS Omega 2022, 7, 42774−42782